Cite This: ACS Appl. Mater. Interfaces XXXX, XXX, XXX–XXX

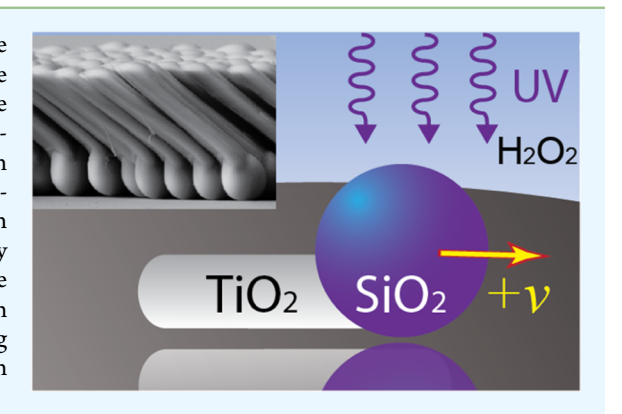
www.acsami.org

# **Shape-Dependent Motion of Structured Photoactive Microswimmers**

Dylan Nicholls, Andrew DeVerse, Ra'Shae Esplin, John Castañeda, Yoseph Loyd, Raaman Nair, Robert Voinescu, <sup>†</sup> Chao Zhou, <sup>‡</sup> Wei Wang, <sup>‡</sup> and John G. Gibbs\*\*, <sup>†</sup>

Supporting Information

ABSTRACT: We investigate the dynamics of structured photoactive microswimmers and show that morphology sensitively determines the swimming behavior. Particular to this study, a major portion of the light-activated particles' underlying structure is built from a photocatalytic material, made possible by dynamic physical vapor deposition (DPVD). We find that swimmers of this type exhibit unique shapedependent autonomous swimming that is distinct from what is seen in systems with similar structural morphology but not fabricated directly from the catalyst. Notably, the direction of motion is a function of these parameters. Because the swimming behavior is strongly correlated with particle shape and material composition, DPVD allows for engineering small-scale propulsion by adjusting the fabrication parameters to match the desired performance.



KEYWORDS: active colloids, active matter, shape-dependent motion, light-activated particles, titanium dioxide, self-propulsion

# ■ INTRODUCTION

Inorganic colloidal particles can be driven in fluids by several means—for example, externally, <sup>1-3</sup> including via the application of a magnetic, <sup>4-10</sup> electric, <sup>11-13</sup> or acoustic field, <sup>14</sup> or active swimmers may self-propel, <sup>15-28</sup> as is the case for the now-famous systems of catalytic nanomotors.<sup>29,30</sup> A method under development involves the use of light activation, 31-46 which offers several advantages including the ability to switch the directed propulsion on and off as well as on-command control over the strength of the activity and therefore particle speed. To date, most photoactive systems introduced consist of simple geometries such as spheres and cylinders, although more complex shapes have been investigated, such as Janus nanotrees.<sup>47</sup> Because morphology strongly influences the motion of self-propelled artificial nano- and microswimmers, 48-50 being able to construct active photocatalytic swimmers with a wider range of geometries is expected to facilitate the targeted engineering of desired autonomous swimming.

In this study, we investigate the effect of shape on the behavior of structured photoactive microswimmers of which a major portion of the underlying structure is made directly from a photocatalytic material. We systematically adjusted the morphology by employing dynamic physical vapor deposition (DPVD)<sup>51-54</sup> and found unique and unexpected modes of motion not seen in comparable systems. For instance, in some cases, we observed that larger structures, with a significantly higher viscous drag, actually moved at the same speed or even faster than their scaled-down smaller counterparts when experimental conditions were identical. We also found that

the direction of motion is a function of a swimmer's shape. Because the motive behavior is quite sensitive to morphological changes, the employed fabrication method allows us to tune the types of motion exhibited by the particles by altering morphology, made possible by modulating the deposition conditions.

We chose to fabricate structured photoactive swimmers from titanium dioxide, TiO2 or titania, because we have found that this material is amenable to forming high-quality nano- and microstructures using oblique-angle DPVD [see Figure 1 for fabrication steps and the resulting scanning electron microscopy (SEM) and energy-dispersive X-ray spectroscopy (EDX) images]. Furthermore, with a band gap of ~3.2 eV, particles made from this material are only catalytically active and are therefore propelled exclusively when light of sufficiently short wavelength ( $\lambda < \sim 390$  nm) is present. We first investigated the dynamics of a simple geometry, SiO<sub>2</sub>/TiO<sub>2</sub> Janus spheres, to characterize our system and to confirm that the dynamics agree at least qualitatively with previously published results, for example ref 34. More specifically, we considered the dependence of speed upon hydrogen peroxide concentration as well as the effect of annealing the particles at different temperatures. As these details are beyond the scope of the present study, which is dedicated to the motion of structured photoactive microswimmers, we refer the reader to the Supporting Information documentation, where in addition to these data the reader may

Received: February 1, 2018 Accepted: May 3, 2018 Published: May 3, 2018

Department of Physics and Astronomy, Northern Arizona University, S San Francisco Street, Flagstaff, Arizona 86011, United States <sup>‡</sup>School of Materials Science and Engineering, Harbin Institute of Technology (Shenzhen), Shenzhen, Guangdong 518055, China

**ACS Applied Materials & Interfaces** 

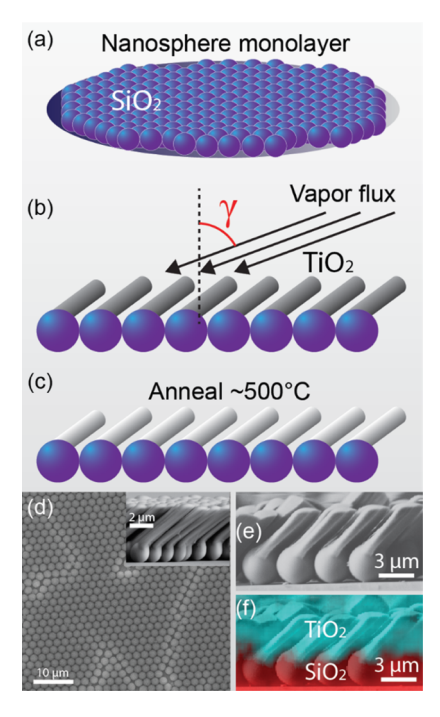


Figure 1. Fabrication of photoactive structured microswimmers (see Materials and Methods for more details). (a) A monolayer of silica particles is first deposited onto a silicon wafer. (b) A thick layer of titania is deposited onto the spheres at an oblique angle  $\gamma$ . (c) After deposition, the structures are annealed at ~500 °C for 3 h. (d) A topdown SEM image of a monolayer of silica spheres of  $\sim$ 2  $\mu$ m in diameter. The inset shows a cross-section image of titania grown atop a similar monolayer, but with an  $SiO_2$  particle of diameter ~1.5  $\mu$ m. (e) A cross-section image showing the resulting oblique angle growth of titania on particles of diameter  $\sim 3.2 \mu m$ . (f) EDX chemical mapping overlaid atop the same image that is given in (e), which shows the location of elemental titanium and silicon as blue/green and red, respectively.

find several videos demonstrating the swimming behaviors of the microswimmers with varying morphology.

#### **RESULTS AND DISCUSSION**

The swimmers, which consist of spherical silica heads and titania tails, settled to a solid surface due to gravity,  $\vec{g}$ , (Figure 2a) and were observed to be moving over that surface (Figure 2b) when exposed to hydrogen peroxide and UV light; the addition of hydrogen peroxide was necessary to observe the propelled motion in this system. Our main goal in this study, investigating how geometry affects motion, was accomplished by altering (1) the length l of the titania tails and (2) the diameter of the spherical head a (see Figure 2b for the definition of these parameters). The particles primarily moved along their axes either toward the tail,  $-\nu$ , or toward the head,  $+\nu$ , shown schematically in Figure 2b and in the video frames of Figure 2c, respectively. Particle speed as a function of tail length for two different constant diameters  $a = 2 \mu m$  and  $a = 3.2 \mu m$  is presented in Figure 3a,b, respectively, for several 10's of particles. Three lengths for the two diameters were investigated, which we refer to as Janus, short-tailed, and long-tailed structures. The insets schematically show the approximate morphology of the microswimmers with different tail lengths, whereas the arrows indicate the direction of motion observed (see Figure 2b for the adopted convention for positive and negative speeds). The average of the absolute value of the

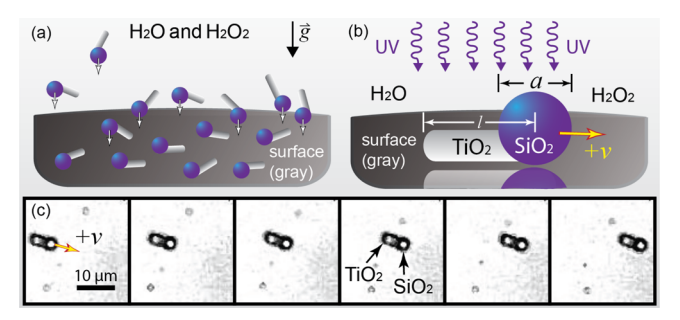
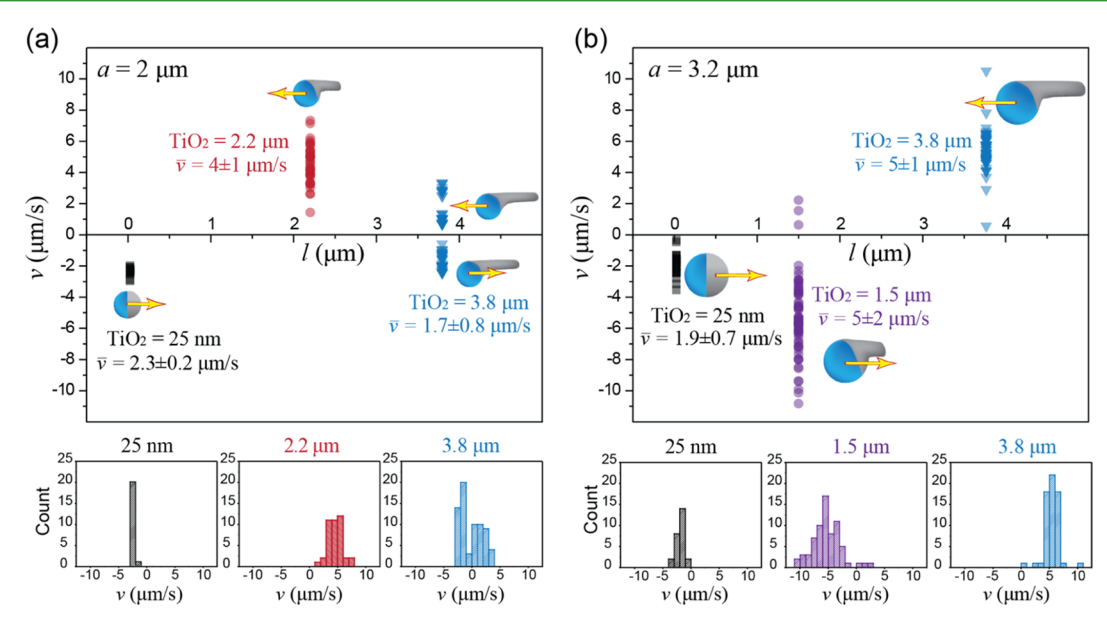


Figure 2. (a) Schematic showing an oblique-angle view of several particles in water and hydrogen peroxide settling to the solid silica surface (gray), which occurs after a droplet of the colloid is placed into an observation cell (see Materials and Methods for details). The particles settle to the bottom of the cell due to gravity,  $\vec{g}$ , and move just above the solid surface. (b) Schematic showing an oblique-angle view of a single swimmer that is activated by UV light. Also shown are the critical dimensions (a, l) and the convention adopted for the positive  $(+\nu)$  direction, which is toward the SiO<sub>2</sub>, or headfirst. The critical dimensions determine which direction the particles move. (c) Example video frames showing the directed motion of a swimmer moving toward the silica head, v > 0. Time increases from left to right in the frames.

speeds,  $\overline{v} = \sum_{i=1}^{N} |v_i|$ , where *i* is the particle index and *N* is the number of data points for a single morphology, is written next to the data points in the plots. Below the main plots are histograms for the distribution of speeds for each morphology.

According to the main plots in Figure 3, the addition of a short photocatalyst tail deposited onto the spherical seed particles, at an oblique angle, significantly increases the average magnitude of the speed in comparison to the Janus spheres. However, we find that for the smaller seed particle (Figure 3a), the direction of motion of the short-tailed structures is exactly opposite the Janus sphere case. That is, all of these swimmers move headfirst, for all speeds v > 0. For the short-tailed structures with the larger seed particle (Figure 3b), this change in the direction of motion has not occurred. We did, however, find that the direction of motion is switched for the long-tailed swimmers that were grown upon the larger seed particle, as shown on the right side of Figure 3b. Thus, switching of the direction of motion was accomplished simply by adding a longer tail to the swimmers, but how long the tail must be depends upon the diameter of the head. We also found that by further increasing the tail length for the smaller seed particle, the speed is reduced and approximately the same number of swimmers move in the positive and negative directions, as shown in Figure 3a. It is possible that if we continued to increase the tail length for the smaller seed particle, we may see a change in the direction of motion once more. However, because increasing the tail length increases drag, we expect that particles with tails longer than  $l = 3.8 \mu m$  would be unlikely to increase in absolute speed. Further, due to the limitations of our deposition system, we were unable to examine the behaviors of swimmers with tail lengths longer than  $\sim$ 4  $\mu$ m.

The data indicate that the short-tailed swimmers with a = 2 $\mu$ m and the long-tailed swimmers with  $a = 3.2 \mu$ m have notable similarities: (1) the particles in both of these particular cases show comparable average speeds,  $\overline{\nu} = 4 \pm 1 \ \mu \text{m/s}$  and  $\overline{\nu} = 5 \pm 1$  $\mu$ m/s for the former and latter, respectively, (2) the particles in both cases move with  $\nu > 0$ , and (3) the proportions of the critical dimensions are similar. If, for simplicity, we make the admittedly very rough approximation that the swimmers are **ACS Applied Materials & Interfaces** 



**Figure 3.** Speed vs length for two different seed particle (head) diameters: (a)  $a = 2 \mu m$  and (b)  $a = 3.2 \mu m$ . Histograms showing the distribution of speeds are given below the main plots and are color-coded corresponding to tail length. The inset schematics show the morphologies corresponding to different head/tail lengths, with arrows indicating the direction of motion along the particle axis. Note that the schematics are on the same scale. The average speeds and tail lengths, in color-coded text, are indicated next to the data points.

cylindrical, then while moving along the axis, the drag at low Reynolds numbers is

$$F_{\rm d} \approx \frac{2\pi \eta l \nu}{\ln\left(\frac{2l}{R}\right) - 0.72} \tag{1}$$

where  $\eta$ , l, R and  $\nu$  are the fluid viscosity, length and radius of the cylinder, and speed, respectively. If we furthermore assume  $\frac{l_2}{R_2} = \frac{l_1}{R_1}$ , which is a reasonable approximation because a/l = 0.91 and 0.84 for the smaller and larger seed particle diameters, respectively, the ratio of the drag force  $F_{\rm d,2}$  of the larger structure to the drag force  $F_{\rm d,1}$  of the smaller structure, when the particles are propelled at the same speed  $\nu$ , is

$$\frac{F_{\rm d,2}}{F_{\rm d,1}} \approx \frac{2\pi\eta l_2 \nu}{\ln\left(\frac{2l_2}{R_2}\right) - 0.72} \left(\frac{2\pi\eta l_1 \nu}{\ln\left(\frac{2l_1}{R_1}\right) - 0.72}\right)^{-1} = \frac{l_2}{l_1}$$
(2)

and thus we find  $\frac{F_{\rm d,2}}{F_{\rm d,1}} \approx$  2. However, we measure the speeds to

be roughly the same under identical experimental conditions, despite the larger structure experiencing twice the drag. We therefore expect the larger particle to be experiencing  $\sim 2\times$  the propulsion. Presently, it is unclear why the particles with parameters  $a=3.2~\mu\text{m},~l=3.8~\mu\text{m}$  would experience greater propulsion in comparison to the smaller  $a=2~\mu\text{m},~l=2.2~\mu\text{m}$  particles, and the observation that the direction of motion is a function of these two parameters a and l is even less clear. We next turn to how these effects potentially arise.

Hong et al. reported active motion of titania particles, but the authors of this paper did not investigate the shape-dependent behavior of these titania-based microswimmers. Further, their particles were not moving in the presence of hydrogen peroxide. The primary findings of that study suggested that multiple mechanisms may be present, and we suspect this to be true in the present study as well. The full description of the mechanism of motion for our system is likely highly complex

because of the added complication of possible shape-dependent flow profiles for asymmetric shapes. However, we will give a qualitative description of a possible mechanism of motion here.

The decomposition of  $H_2O_2$  occurs at the  $TiO_2$  surface via two possible reactions

$$H_2O_2 + 2e^- + 2H^+ \rightarrow 2H_2O$$
 (3)

$$H_2O_2 + 2h^+ \rightarrow O_2 + 2H^+$$
 (4)

which are facilitated by UV-light-induced electron—hole generation on the surface of the anatase TiO<sub>2</sub> segments of the active particles. A proposed mechanism for the TiO<sub>2</sub>/SiO<sub>2</sub> active Janus sphere in H<sub>2</sub>O<sub>2</sub> was presented by Singh et al.<sup>34</sup> A local chemical gradient of products, for example O<sub>2</sub>, and/or reactants develops. Based upon the observed direction of motion, we speculate that these concentration gradients lead to a fluid flow from the TiO<sub>2</sub> toward the SiO<sub>2</sub> surface, shown by the curved arrows in Figure 4, which in turn leads to the particle being propelled in the opposite direction (Figure 5a). However, in the cited study, the particles investigated were Janus spheres only. Particles with more complex shapes, such as those presented herein, are expected to have significantly

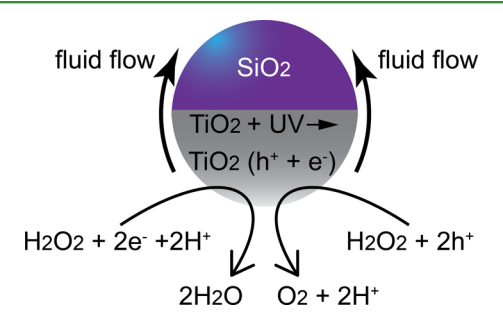


**Figure 4.** Schematic showing the possible mechanism of motion for a  $TiO_2/SiO_2$  Janus sphere in  $H_2O_2$ . A chemical gradient develops from the photocatalyzed reaction and leads to a flow from the reaction site to the  $SiO_2$  hemisphere.

**ACS Applied Materials & Interfaces** 

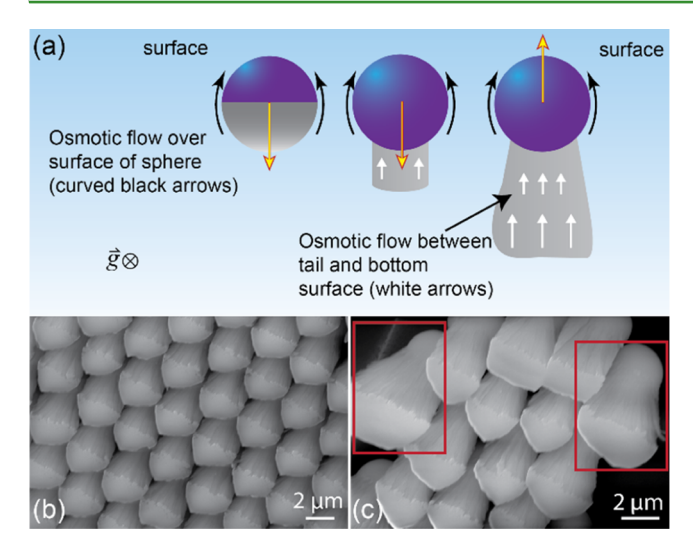


Figure 5. (a) Potential mechanism for the dependence of the direction of motion with increasing tail length. Osmotic flow over the silica sphere is present in all three cases and is indicated by the curved black arrows. The direction of motion is indicated by straight yellow arrows with red outline. Osmotic flow between the surface of the bottom of the observation cell and the particles is indicated by white arrows. Note that in this top-down view, this flow is underneath the titania tail. (b) Top-down SEM image showing titania tail growth on a defect-free segment of the colloidal crystal. (c) The red boxes show the exaggerated broadening of the tails near the edges of the crystal.

different flow profiles. It should be noted that the flow may be a result of a concentration gradient of charged species as well.<sup>55</sup>

To further delve into the possible effects of shape on the observations herein, we present a schematic in Figure 5a that shows three cases from left to right: the Janus sphere, short tail, and long tail swimmers. The orientation of the schematic is topdown, and the active particles are being propelled in the direction of the straight yellow arrows with a red outline, consistent with the observed directions of motion. As indicated in Figure 5, the flow over the surface of the particle toward the SiO<sub>2</sub> face, represented by the curved black arrows for all three cases, leads to propulsion opposite to this flow, that is motion toward the titania.<sup>34</sup> For the structured swimmers with short tails, there may develop a stronger gradient in comparison to the Janus sphere case, and consequently, a larger flow, simply because of the larger surface area of the catalyst. With a larger gradient, we expect an enhanced speed as  $v \propto \nabla c$ , where c is the concentration field surrounding the particle.<sup>56</sup> Therefore, particles with the morphology  $a = 3.2 \mu m$ ,  $l = 3.8 \mu m$  would experience greater propulsion in comparison to the smaller a =2  $\mu$ m,  $l = 2.2 \mu$ m particles, which is consistent with our observations.

So why would the direction of motion be a function of the two parameters l and a? Intuitively, a first guess would be that competing mechanisms are present, but which dominates depends upon the geometry of the swimmer. Because a swimmer moves close to a wall (bottom surface), the concentration gradients that develop around the swimmers may generate chemi-osmotic flow on the stationary surface, which has been suggested to couple back to the particle affecting its motion. 57 For example, it has been suggested that the motion of photoactive swimmers is in part a result of "surfing" on such osmotic flow between the particle and the surface over which it moves, as discussed by Palacci et al.<sup>35</sup> If the portion of this flow between the stationary bottom surface

and the tail of the mobile particle, represented by the white arrows in Figure 5a, is asymmetric, then a net movement is expected. For the fabrication process used, the length and width of the tail mutually increase or the tail broadens as it increases in length, 58 as shown on the right side of Figure 5a. Thus, a stronger concentration gradient is expected to develop near the end of the particle, where the surface area of the catalyst is larger, potentially leading to an asymmetric osmotic flow toward the silica head upon which the particle could move (white arrows). In essence, two competing mechanisms work to drive the particles in opposite directions: self-phoresis leading to motion toward the tail and osmotic "surfing" leading to motion toward the head. Which mechanism dominates in this case would then be a function of the morphology. We note that the full description of the mechanism for photocatalytic active systems is lacking in the literature, and the mechanism is likely to be multifaceted especially for particles with complex or asymmetric shapes as asymmetry will inevitably alter flow and thus the propulsion. An example study investigated "peanut"shaped particles made from hematite that showed ~75% moving from the larger side to the smaller. 40 These swimmers being isotropic with respect to the material, the asymmetry of the shape alone gives rise to self-propulsion, whereas in our system we have both shape and material anisotropy.

To briefly investigate the effects of asymmetry in our system, we look at a special case in which the previously mentioned tail broadening is greatly exaggerated. With greater broadening, it is possible, considering the toy model in Figure 5, that a larger asymmetry in the osmotic flow between the particle and the substrate would be present, and thus we should observe higher speeds. We found several such structures in our experiments, which result from the DPVD process combined with the location of the seed particle during deposition. If a sphere is situated in a way so that the titania is not shadowed by adjacent spheres, the broadening of the titania tail is much greater as demonstrated in the SEM images of Figure 5b,c. The image in Figure 5b shows "narrow" titania tails grown upon close-packed spheres. However, if spheres were to reside at the edge of a domain, tail growth on such spheres will show significantly greater broadening. The structures outlined with red rectangles atop the SEM image of Figure 5c shows this effect. We find that these particles, in general, move at speeds significantly higher than their more symmetric counterparts, which is expected because more asymmetry should lead to higher asymmetric osmotic flow. As a quick comparison, we revisit the  $a = 2 \mu m$ , l=  $2.2 \mu m$  case. Because the broadening is so severe, by visual discrimination of the particles in the videos alone, we can easily distinguish the broad tails from the narrow tails, and we found speeds of  $\overline{v} = 6 \pm 2 \ \mu \text{m/s}$  for the former and  $\overline{v} = 3 \pm 1 \ \mu \text{m/s}$  for the latter, or the broad-tailed swimmers move  $\sim$ 2× faster than their narrow counterparts. Video S4 in the Supporting Information demonstrates this effect.

## **CONCLUSIONS**

We have fabricated and investigated the morphology-dependent behavior of structured photoactive microswimmers that were constructed directly from the catalyst itself. For microswimmers with photocatalytic tails, we found that both the tail length and the diameter of the head have significant effects upon the types of swimming behaviors observed. We found that by altering the length of the photocatalytic tail, swimming speed and even the direction of motion change. The ratio of the diameter of a swimmer's head to the length of the

tail appears to be the governing parameter. For instance, when these two main critical dimensions, tail length and head diameter, are approximately the same, we find that the direction of motion is opposite that observed in the Janus sphere case. Thus, by tuning the geometry and constructing photocatalytic microswimmers directly from the catalyst material itself, we are able to modulate the swimming behavior significantly. The system herein may open up new possible research directions. For example, the control over the direction of motion could allow for investigating interesting effects regarding the collective behavior of a large number of interacting active swimmers. For instance, it was shown numerically that particles of similar geometry moving in opposite directions show phase separation.<sup>59</sup> The system herein could make experimental investigations of such phenomena realizable.

#### MATERIALS AND METHODS

The steps leading to the fabrication and actuation of the swimmers are illustrated in Figure 1. Shown in Figure 1a, monolayers of SiO<sub>2</sub> microspheres were deposited onto Si(100) wafers, which were precleaned with oxygen plasma, either with a Langmuir-Blodgett method or by simple drop-casting. Two diameters of SiO<sub>2</sub> beads were used (2.0 and 3.2  $\mu$ m) to investigate size-dependent effects. The SiO<sub>2</sub> spheres served as a nucleation template for the DPVD technique known as glancing angle deposition.  $^{52,53}$  The deposition of TiO<sub>2</sub> was performed at an oblique angle of  $\gamma = 85^{\circ}$  with respect to the evaporation source, as shown in Figure 1b. Approximately columnar tails of TiO2 were grown to various lengths by employing electronbeam evaporation at a vacuum pressure of  $P \le 2.0 \times 10^{-5}$  Torr. After deposition, the substrates were removed from the deposition chamber and annealed in a Thermolyne 21100 Furnace at ~500 °C for 3 h (see Figure 1c) to obtain primarily the anatase phase of titania. The structures were detached from the surface, separated from the array, and dispersed into pure water using gentle bath sonication.

The microswimmers were observed to be moving within an observation cell made the following way: we first cut a square hole from a piece of double-sided tape. The tape was adhered to an oxygenplasma-cleaned silica microscope slide, and, to keep the fluid at the center of the cell, a hydrophobic PAP pen was employed to draw a hydrophobic square-shaped ring on the slide along the inner edge of the tape. A droplet of water that contained the particles, followed by an additional droplet of hydrogen peroxide, was pipetted into the cell, which was then sealed using a clean glass cover slide. The concentration of hydrogen peroxide in all experiments was held constant at 1% (v/v), even though our experiments indicate that concentration has little effect on speed in this system (see Supporting Information). The swimmers settled to the surface of the glass slide at the bottom of the cell (see Figure 2a). A fluorescence microscope (Zeiss AxioScope.A1) was used to observe their motion under brightfield illumination, whereas a light emitting diode UV light source  $(\lambda = 365 \text{ nm})$  was used for activation. The intensity of the UV light was uniform in all experiments at a value of ~2 W/cm<sup>2</sup>. Once activated, the particles moved just above the bottom surface of the cell, typically along their major axis. The length is defined as the distance from the center of the sphere to the end of the tail, as shown in Figure 2b, which we measured with a Zeiss Supra 40VP scanning electron microscope. Characterization was performed using SEM and a Thermo Scientific EDX at the Imaging and Histology Core Facility at Northern Arizona University. Videos of the microswimmers were recorded with a Mikrotron EoSens GE MC1364 camera at a frame rate of 10 fps, and the motion was analyzed using the plugin MTrack2 for the software ImageJ. Several videos are provided in the Supporting Information.

Example arrays of the structures resulting from the fabrication process, described schematically in Figure 1a-c, can be found in Figure 1d-f. Shown in Figure 1d is a top-down image of a monolayer of silica spheres  $\sim 2 \mu m$  in diameter. On average, we found the structures to be qualitatively of high uniformity. An example can be

seen in Figure 1e, which shows a cross-section SEM image of silica microspheres of  $\sim 3.2 \mu m$  diameter with attached approximately columnar tails of  $TiO_2$  which was deposited at an oblique angle of  $\gamma =$ 85° (see Figure 1b for the definition of  $\gamma$ ). Figure 1f shows a chemical map, obtained with EDX, overlaying the same image in Figure 1e. The map shows the location of elemental silicon (red) at the bottom and elemental titanium (blue/green) at the top, consistent with expectations. Note that the inset SEM image in Figure 1d and the image in Figure 1e are on the same scale.

#### ASSOCIATED CONTENT

# Supporting Information

The Supporting Information is available free of charge on the ACS Publications website at DOI: 10.1021/acsami.8b01940.

> See supporting information for videos of the photoactive particles and a document describing additional experiments, procedures, and methods (PDF)

> 3.2  $\mu$ m-diameter Janus spheres moving in 1% H<sub>2</sub>O<sub>2</sub> (V/ V) under UV illumination (AVI)

> Short-tailed ( $a = 3.2 \mu \text{m}$  and  $l = 1.5 \mu \text{m}$ ) structured swimmers in 1% H<sub>2</sub>O<sub>2</sub> (V/V) (AVI)

> Long-tailed ( $a = 3.2 \mu m$  and  $l = 3.8 \mu m$ ) structured swimmers in 1% H<sub>2</sub>O<sub>2</sub> (V/V) under UV illumination

> Demonstration of broad-tailed swimmers moving faster than their narrow counterparts for the  $a = 2 \mu m$  and l = $2.2 \mu m$  morphology (AVI)

#### AUTHOR INFORMATION

#### **Corresponding Author**

\*E-mail: john.gibbs@nau.edu.

ORCID ®

John G. Gibbs: 0000-0002-6510-9352

## **Author Contributions**

This manuscript was written primarily by D.N., W.W., & J.G.G., but also through contributions of all other authors, all of whom have approved the final version.

#### **Notes**

The authors declare no competing financial interest.

### ACKNOWLEDGMENTS

This material is based upon work supported by the National Science Foundation under grant no. CBET-1703322, and was also supported in part by the State of Arizona Technology and Research Initiative Fund (TRIF), administered by the Arizona Board of Regents (ABOR). We would also like to thank the Imaging and Histology Core Facility at Northern Arizona University for their assistance with optical and electron microscopy. In particular, we give special thanks to Aubrey Funke for her invaluable assistance with these instruments.

#### **REFERENCES**

- (1) Shields, C. W.; Veley, O. D. The Evolution of Active Particles: Toward Externally Powered Self-Propelling and Self-Reconfiguring Particle Systems. Chem 2017, 3, 539-559.
- (2) Jiang, H.-R.; Yoshinaga, N.; Sano, M. Active Motion of a Janus Particle by Self-Thermophoresis on a Defocused Laser Beam. Phys. Rev. Lett. 2010, 105, 268302.
- (3) Kim, J. T.; Choudhury, U.; Jeong, H.-H.; Fischer, P. Nanodiamonds that Swim. Adv. Mater. 2017, 29, 1701024.
- (4) Schamel, D.; Pfeifer, M.; Gibbs, J. G.; Miksch, B.; Mark, A. G.; Fischer, P. Chiral Colloidal Molecules and Observation of the Propeller Effect. J. Am. Chem. Soc. 2013, 135, 12353-12359.

- (5) Vach, P. J.; Brun, N.; Bennet, M.; Bertinetti, L.; Widdrat, M.; Baumgartner, J.; Klumpp, S.; Fratzl, P.; Faivre, D. Selecting for Function: Solution Synthesis of Magnetic Nanopropellers. *Nano Lett.* **2013**, *13*, 5373–5378.
- (6) Schamel, D.; Mark, A. G.; Gibbs, J. G.; Miksch, C.; Morozov, K. I.; Leshansky, A. M.; Fischer, P. Nanopropellers and their Actuation in Complex Viscoelastic Media. *ACS Nano* **2014**, *8*, 8794–8801.
- (7) Venugopalan, P. L.; Sai, R.; Chandorkar, Y.; Basu, B.; Shivashankar, S.; Ghosh, A. Conformal Cytocompatible Ferrite Coatings Facilitate the Realization of a Nanovoyager in Human Blood. *Nano Lett.* **2014**, *14*, 1968–1975.
- (8) Walker, D.; Kübler, M.; Morozov, K. I.; Fischer, P.; Leshansky, A. M. Optimal Length of Low Reynolds Number Nanopropellers. *Nano Lett.* **2015**, *15*, 4412–4416.
- (9) Jeong, H.-H.; Mark, A. G.; Lee, T.-C.; Alarcón-Correa, M.; Eslami, S.; Qiu, T.; Gibbs, J. G.; Fischer, P. Active Nanorheology with Plasmonics. *Nano Lett.* **2016**, *16*, 4887–4894.
- (10) García-Torres, J.; Serrà, A.; Tierno, P.; Alcobé, X.; Vallés, E. Magnetic Propulsion of Recyclable Catalytic Nanocleaners for Pollutant Degradation. ACS Appl. Mater. Interfaces 2017, 9, 23859—23868.
- (11) Wang, S.; Ma, F.; Zhao, H.; Wu, N. Bulk Synthesis of Metal—Organic Hybrid Dimers and Their Propulsion under Electric Fields. *ACS Appl. Mater. Interfaces* **2014**, *6*, 4560–4569.
- (12) Xu, X.; Kim, K.; Fan, D. Tunable Release of Multiplex Biochemicals by Plasmonically Active Rotary Nanomotors. *Angew. Chem., Int. Ed.* **2015**, *54*, 2525–2529.
- (13) Kim, K.; Guo, J.; Xu, X.; Fan, D. Micromotors with Step-Motor Characteristics by Controlled Magnetic Interactions among Assembled Components. ACS Nano 2015, 9, 548–554.
- (14) Li, J.; Li, T.; Xu, T.; Kiristi, M.; Liu, W.; Wu, Z.; Wang, J. Magneto-Acoustic Hybrid Nanomotor. *Nano Lett.* **2015**, *15*, 4814–4821.
- (15) Sánchez, S.; Soler, L.; Katuri, J. Chemically Powered Micro-and Nanomotors. *Angew. Chem., Int. Ed.* **2015**, *54*, 1414–1444.
- (16) Lee, T.-C.; Alarcón-Correa, M.; Miksch, C.; Hahn, K.; Gibbs, J. G.; Fischer, P. Self-propelling Nanomotors in the Presence of Strong Brownian Forces. *Nano Lett.* **2014**, *14*, 2407–2412.
- (17) Wu, Y.; Lin, X.; Wu, Z.; Möhwald, H.; He, Q. Self-Propelled Polymer Multilayer Janus Capsules for Effective Drug Delivery and Light-Triggered Release. ACS Appl. Mater. Interfaces 2014, 6, 10476—10481.
- (18) Vilela, D.; Stanton, M. M.; Parmar, J.; Sánchez, S. Microbots Decorated with Silver Nanoparticles Kill Bacteria in Aqueous Media. *ACS Appl. Mater. Interfaces* **2017**, *9*, 22093–22100.
- (19) Claussen, J. C.; Daniele, M. A.; Geder, J.; Pruessner, M.; Mäkinen, A. J.; Melde, B. J.; Twigg, M.; Verbarg, J. M.; Medintz, I. L. Platinum-paper micromotors: An Urchin-Like Nanohybrid Catalyst for Green Monopropellant Bubble-Thrusters. ACS Appl. Mater. Interfaces 2014, 6, 17837–17847.
- (20) Sundararajan, S.; Lammert, P. E.; Zudans, A. W.; Crespi, V. H.; Sen, A. Catalytic Motors for Transport of Colloidal Cargo. *Nano Lett.* **2008**, *8*, 1271–1276.
- (21) He, Y.; Wu, J.; Zhao, Y. Designing Catalytic Nanomotors by Dynamic Shadowing Growth. *Nano Lett.* **2007**, *7*, 1369–1375.
- (22) Nourhani, A.; Brown, D.; Pletzer, N.; Gibbs, J. G. Engineering Contactless Particle—Particle Interactions in Active Microswimmers. *Adv. Mater.* **2017**, *29*, 1703910.
- (23) Johnson, J. N.; Nourhani, A.; Peralta, R.; McDonald, C.; Thiesing, B.; Mann, C. J.; Lammert, P. E.; Gibbs, J. G. Dynamic Stabilization of Janus Sphere Trans-Dimers. *Phys. Rev. E* **2017**, 95, 042609.
- (24) Ma, X.; Jannasch, A.; Albrecht, U.-R.; Hahn, K.; Miguel-López, A.; Schäffer, E.; Sánchez, S. Enzyme-Powered Hollow Mesoporous Janus Nanomotors. *Nano Lett.* **2015**, *15*, 7043–7050.
- (25) Li, J.; Shklyaev, O. E.; Li, T.; Liu, W.; Shum, H.; Rozen, I.; Balazs, A. C.; Wang, J. Self-Propelled Nanomotors Autonomously Seek and Repair Cracks. *Nano Lett.* **2015**, *15*, 7077–7085.

- (26) Choudhury, U.; Soler, L.; Gibbs, J. G.; Sanchez, S.; Fischer, P. Surface Roughness-Induced Speed Increase for Active Janus Micromotors. *Chem. Commun.* **2015**, *51*, 8660–8663.
- (27) Gibbs, J. G.; Fischer, P. Active Colloidal Microdrills. Chem. Commun. 2015, 51, 4192–4195.
- (28) Jang, B.; Wang, W.; Wiget, S.; Petruska, A. J.; Chen, X.; Hu, C.; Hong, A.; Folio, D.; Ferreira, A.; Pané, S.; Nelson, B. J. Catalytic Locomotion of Core—Shell Nanowire Motors. *ACS Nano* **2016**, *10*, 9983—9991.
- (29) Paxton, W. F.; Kistler, K. C.; Olmeda, C. C.; Sen, A.; St. Angelo, S. K.; Cao, Y.; Mallouk, T. E.; Lammert, P. E.; Crespi, V. H. Catalytic Nanomotors: Autonomous Movement of Striped Nanorods. *J. Am. Chem. Soc.* **2004**, *126*, 13424–13431.
- (30) Wang, Y.; Hernandez, R. M.; Bartlett, D. J.; Bingham, J. M.; Kline, T. R.; Sen, A.; Mallouk, T. E. Bipolar Electrochemical Mechanism for the Propulsion of Catalytic Nanomotors in Hydrogen Peroxide Solutions. *Langmuir* **2006**, *22*, 10451–10456.
- (31) Palacci, J.; Sacanna, S.; Steinberg, A. P.; Pine, D. J.; Chaikin, P. M. Living Crystals of Light-Activated Colloidal Surfers. *Science* **2013**, 339, 936–940.
- (32) Dong, R.; Zhang, Q.; Gao, W.; Pei, A.; Ren, B. Highly Efficient Light-Driven TiO2—Au Janus Micromotors. ACS Nano 2016, 10, 839—844
- (33) Zhang, Q.; Dong, R.; Wu, Y.; Gao, W.; He, Z.; Ren, B. Light-Driven Au-WO3@C Janus Micromotors for Rapid Photodegradation of Dye Pollutants. ACS Appl. Mater. Interfaces 2017, 9, 4674—4683.
- (34) Singh, D. P.; Choudhury, U.; Fischer, P.; Mark, A. G. Non-Equilibrium Assembly of Light-Activated Colloidal Mixtures. *Adv. Mater.* **2017**, *29*, 1701328.
- (35) Palacci, J.; Sacanna, S.; Kim, S.-H.; Yi, G.-R.; Pine, D. J.; Chaikin, P. M. Light-Activated Self-Propelled Colloids. *Philos. Trans. R. Soc., A* **2014**, 372, 20130372.
- (36) Jang, B.; Hong, A.; Kang, H. E.; Alcantara, C.; Charreyron, S.; Mushtaq, F.; Pellicer, E.; Büchel, R.; Sort, J.; Lee, S. S.; Nelson, B. J.; Pané, S. Multiwavelength Light-Responsive Au/B-TiO2 Janus Micromotors. ACS Nano 2017, 11, 6146–6154.
- (37) Wang, J.; Xiong, Z.; Zhan, X.; Dai, B.; Zheng, J.; Liu, J.; Tang, J. A Silicon Nanowire as a Spectrally Tunable Light-Driven Nanomotor. *Adv. Mater.* **2017**, *29*, 1701451.
- (38) Chen, C.; Mou, F.; Xu, L.; Wang, S.; Guan, J.; Feng, Z.; Wang, Q.; Kong, L.; Li, W.; Wang, J.; Zhang, Q. Light-Steered Isotropic Semiconductor Micromotors. *Adv. Mater.* **2017**, *29*, 1603374.
- (39) Zhou, D.; Li, Y. C.; Xu, P.; Ren, L.; Zhang, G.; Mallouk, T. E.; Li, L. Visible-light driven Si–Au Micromotors in Water and Organic Solvents. *Nanoscale* **2017**, *9*, 11434–11438.
- (40) Lin, Z.; Si, T.; Wu, Z.; Gao, C.; Lin, X.; He, Q. Light-Activated Active Colloid Ribbons. *Angew. Chem., Int. Ed.* **2017**, *56*, 13517–13520.
- (41) Ibele, M.; Mallouk, T. E.; Sen, A. Schooling Behavior of Light-Powered Autonomous Micromotors in Water. *Angew. Chem., Int. Ed.* **2009**, *48*, 3308–3312.
- (42) Gao, Y.; Mou, F.; Feng, Y.; Che, S.; Li, W.; Xu, L.; Guan, J. Dynamic Colloidal Molecules Maneuvered by Light-Controlled Janus Micromotors. *ACS Appl. Mater. Interfaces* **2017**, *9*, 22704–22712.
- (43) Zhang, Q.; Dong, R.; Chang, X.; Ren, B.; Tong, Z. Spiropyran-Decorated SiO2–Pt Janus Micromotor: Preparation and Light-Induced Dynamic Self-Assembly and Disassembly. *ACS Appl. Mater. Interfaces* **2015**, *7*, 24585–24591.
- (44) Feldmann, D.; Maduar, S. R.; Santer, M.; Lomadze, N.; Vinogradova, O. I.; Santer, S. Manipulation of Small Particles at Solid Liquid Interface: Light Driven Diffusioosmosis. *Sci. Rep.* **2016**, *6*, 36443
- (45) Zhou, D.; Li, Y. C.; Xu, P.; McCool, N. S.; Li, L.; Wang, W.; Mallouk, T. E. Visible-Light Controlled Catalytic Cu2O—Au Micromotors. *Nanoscale* **2017**, *9*, 75–78.
- (46) Xuan, M.; Wu, Z.; Shao, J.; Dai, L.; Si, T.; He, Q. Near Infrared Light-Powered Janus Mesoporous Silica Nanoparticle Motors. *J. Am. Chem. Soc.* **2016**, *138*, 6492.

- (47) Dai, B.; Wang, J.; Xiong, Z.; Zhan, X.; Dai, W.; Li, C.-C.; Feng, S.-P.; Tang, J. Programmable Artificial Phototactic Microswimmer. *Nat. Nanotechnol.* **2016**, *11*, 1087–1092.
- (48) Gibbs, J. G.; Kothari, S.; Saintillan, D.; Zhao, Y.-P. Geometrically Designing the Kinematic Behavior of Catalytic Nanomotors. *Nano Lett.* **2011**, *11*, 2543–2550.
- (49) Lugli, F.; Brini, E.; Zerbetto, F. Shape Governs the Motion of Chemically Propelled Janus Swimmers. *J. Phys. Chem. C* **2012**, *116*, 592–598.
- (50) Nourhani, A.; Lammert, P. E. Geometrical Performance of Self-Phoretic Colloids and Microswimmers. *Phys. Rev. Lett.* **2016**, *116*, 178302.
- (51) Jeong, H.-H.; Mark, A. G.; Gibbs, J. G.; Reindl, T.; Waizmann, U.; Weis, J.; Fischer, P. Shape Control in Wafer-Based Aperiodic 3D Nanostructures. *Nanotechnology* **2014**, *25*, 235302.
- (52) Mark, A. G.; Gibbs, J. G.; Lee, T.-C.; Fischer, P. Hybrid Nanocolloids with Programmed Three-Dimensional Shape and Material Composition. *Nat. Mater.* **2013**, *12*, 802–807.
- (53) Hawkeye, M. M.; Brett, M. J. Glancing Angle Deposition: Fabrication, Properties, and Applications of Micro-and Nanostructured Thin Films. J. Vac. Sci. Technol., A 2007, 25, 1317.
- (54) Zhao, Y.; Ye, D.; Wang, G.-C.; Lu, T.-M. Designing Nanostructures by Glancing Angle Deposition. *Proceedings Volume* 5219, Nanotubes and Nanowires, 2003; pp 59–73.
- (55) Hong, Y.; Diaz, M.; Córdova-Figueroa, U. M.; Sen, A. Light-Driven Titanium-Dioxide-Based Reversible Microfireworks and Micromotor/Micropump Systems. *Adv. Funct. Mater.* **2010**, *20*, 1568.
- (56) Theurkauff, I.; Cottin-Bizonne, C.; Palacci, J.; Ybert, C.; Bocquet, L. Dynamic Clustering in Active Colloidal Suspensions with Chemical Signaling. *Phys. Rev. Lett.* **2012**, *108*, 268303.
- (57) Popescu, M. N.; Uspal, W. E.; Dietrich, S. Chemically Active Colloids Near Osmotic-Responsive Walls with Surface-Chemistry Gradients. *J. Phys.: Condens. Matter* **2017**, *29*, 134001.
- (58) Kesapragada, S. V.; Gall, D. Anisotropic Broadening of Cu Nanorods During Glancing Angle Deposition. *Appl. Phys. Lett.* **2006**, 89, 203121.
- (59) Wensink, H. H.; Kantsler, V.; Goldstein, R. E.; Dunkel, J. Controlling Active Self-Assembly Through Broken Particle-Shape Symmetry. *Phys. Rev. E: Stat., Nonlinear, Soft Matter Phys.* **2014**, 89, No. 010302(R).